

# Supporting Information

## Construction of Three-Dimensionally Ordered Macroporous Bimetal Phosphides as Bifunctional Electrocatalysts for Highly Efficient Water Splitting

Jianying Wang, Yanli Niu, Xue Teng, Shuaiqi Gong, Jiahui Huang, Mingze Xu and Zuofeng  
Chen\*

Shanghai Key Lab of Chemical Assessment and Sustainability, School of Chemical Science  
and Engineering, Tongji University, Shanghai 200092, China

## Experimental

**Chemicals.** Methyl methacrylate ( $C_5H_8O_2$ , 99%), potassium peroxodisulfate ( $K_2S_2O_8$ , 99.5%), ethyleneglycol ( $CH_2(OH)_2$ , 98%), methanol ( $CH_3OH$ , 99.5%), iron nitrate ( $Fe(NO_3)_3 \cdot 9H_2O$ , 98.5%), nickel nitrate ( $Ni(NO_3)_2 \cdot 6H_2O$ , 98%), cobalt nitrate ( $Co(NO_3)_2 \cdot 6H_2O$ , 99%), and sodium hypophosphite ( $NaH_2PO_2$ , 99%) were all purchased from Macklin Biochemical Co., Ltd. The 1 M KOH solution was purchased from Shanghai Aladdin Biochemical Technology Co., Ltd. All reagents were used as received without further purification. The water solutions were prepared with deionized water ( $18\text{ M}\Omega \cdot \text{cm}$ ) unless stated otherwise.

**Synthesis of PMMA Colloidal Crystal Template.** Monodisperse polymethyl methacrylate (PMMA) spheres were synthesized by an emulsifier-free emulsion polymerization method. Firstly, 0.8 g potassium peroxodisulfate was added into 1500 mL water under the condition of stirring at 400 rpm and flowing nitrogen gas. After equilibrating to 70 °C, 115 mL methyl methacrylate monomer was poured into the flask and stirred at the temperature for 1 hour. The PMMA colloidal crystal spheres were separated from the as-prepared colloidal suspension by centrifugation (4000 rpm). The supernatant was removed and the precipitate was washed for three times using deionized water. Then, the precipitate was dispersed into deionized water by ultrasonic treatment and the colloidal suspension was poured into a small beaker followed by evaporating in a water bath at 80 °C. The as-obtained PMMA colloidal crystal template was stored in a sealed glass container.

**Synthesis of 3DOM Bimetal Oxides.** A certain amount of  $Fe(NO_3)_3$  and  $Ni(NO_3)_2$  was dissolved in 8 mL ethyleneglycol in a beaker by stirring at room temperature for 6 h. The total concentration of the metal ions was 2 mol/L. Then, 5 mL methanol was added in the above solution. After stirring for 12 h, 2 g PMMA colloidal crystals were poured into the solution and soaked for two days. The impregnated PMMA colloidal crystals were separated from the

excessive solution by vacuum filtration. Finally, the 3DOM metal oxides were obtained by pyrolysis of the impregnated PMMA colloidal crystals in a tubular furnace at an air flow of 120 mL/min. The temperature was raised at a ramping rate of 1 °C /min to 350 °C and held for 3 h. The 3DOM oxides with different Ni:Fe (3:1, 1:1, 1:3) were fabricated by adjusting the feeding molar ratio of  $\text{Fe}(\text{NO}_3)_3$  and  $\text{Ni}(\text{NO}_3)_2$ . As reference, the single nickel and iron oxides were prepared by the same method. In addition, the 3DOM CoFe oxide with the molar ratio of Fe:Co = 1:1 was also prepared with the assistance of PMMA template.

***Synthesis of 3DOM Bimetal Phosphides.*** The 3DOM bimetal phosphides were prepared by the solid-phase phosphorization method. The as-prepared 3DOM NiFe oxides were put in the downstream and  $\text{NaH}_2\text{PO}_2$  as P source in the upstream in an atmosphere of argon in the tubular furnace. The temperature was raised at a ramping rate of 3 °C/min to 350 °C and held for 2 h. The as-prepared metal phosphides were stored in a sealed glass container filled with inert argon gas for further characterization and testing.

***Characterization.*** Scanning electron microscopy (SEM) images, energy dispersive X-ray spectroscopy data (EDX) and EDX mapping images were obtained at Hitachi S-4800 (Hitachi, Japan) equipped with a Horiba EDX system (X-max, silicon drift X-Ray detector). Transmission electron microscopy (TEM) images, high resolution TEM (HRTEM) images and selected area electron diffraction (SAED) image were obtained using Tecnai G2 F20 S-Twin. Powder X-ray diffraction (XRD) was measured by Bruker D8 Focus via ceramic monochromatized  $\text{Cu K}\alpha$  radiation of 1.54178 Å, operating at 40 kV and 40 mA. The scanning range was from 30 - 60°. X-ray photoelectron spectroscopy (XPS) for elemental analysis was conducted on a Kratos Axis Ultra DLD X-ray Photoelectron Spectrometer using 60 W monochromated  $\text{Al K}\alpha$  radiation as the X-ray source for excitation. The carbon 1s peak (284.6 eV) was used for internal calibration. The peak resolution and fitting were processed by XPS Peak 41 software. Surface area measurements were performed on an ASAP 2020 Brunauer-

Emmett-Teller (BET) instrument. The water contact angle value was obtained by averaging five measurements at different positions on the same sample with a constant volume of water (4  $\mu\text{L}$ ) via a Dataphysics OCT-20 contact-angle system. Thermogravimetry (TG) measurement was carried out on a thermal analyzer (TGA Q500), and the samples were heated at a rate of 1  $^{\circ}\text{C}/\text{min}$  in an air flow. Thermal analysis was carried out with differential scanning calorimetry apparatus (TA Instrument DSC Q2000).

***Electrochemical Measurements.*** The working electrode was prepared by the following steps: Firstly, 4 mg of the as-prepared electrocatalyst material and 80  $\mu\text{l}$  of 5 wt% Nafion solution were dispersed in 1 ml of water/ethanol solution by sonication treatment. Then, 5  $\mu\text{L}$  of the electrocatalyst suspension was dropped onto the glassy carbon electrode (mass loading  $\sim 0.265 \text{ mg cm}^{-2}$ ) and dried at room temperature to obtain the working electrode for electrochemical measurements.

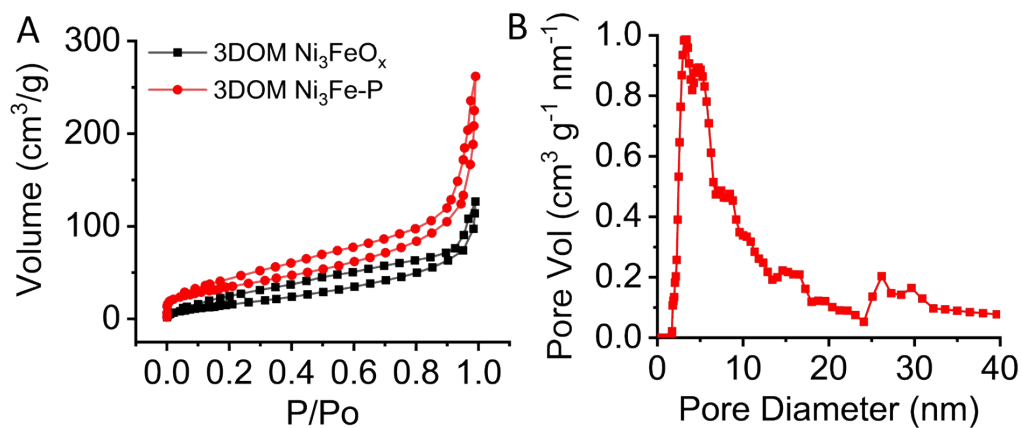
All electrochemical measurements were performed on a CHI 660E electrochemical workstation (Chenhua Corp., Shanghai, China). The three-electrode system consisted of a working electrode, a carbon rod counter electrode, and a saturated calomel reference electrode (SCE,  $\sim 0.244 \text{ V vs. NHE}$ ). Unless stated otherwise, all potentials in linear sweep voltammetric (LSV) curves by the three-electrode setup were reported vs. RHE with 90%  $iR$  compensation and all controlled potential electrolysis (CPE) experiments were conducted without  $iR$  compensation. All experiments were performed at  $22 \pm 2 \text{ }^{\circ}\text{C}$ .

***Tafel plot.*** The current-potential data of the electrocatalysts were obtained by linear sweep voltammetry (LSV) at a very slow scan rate of 0.1 mV/s. The Tafel slope was obtained from the LSV plot using a linear fit applied to points in the Tafel region. The solution resistance measured prior to the data collection (using  $iR$  test function) was used to correct the Tafel plot for the  $iR$  drop.

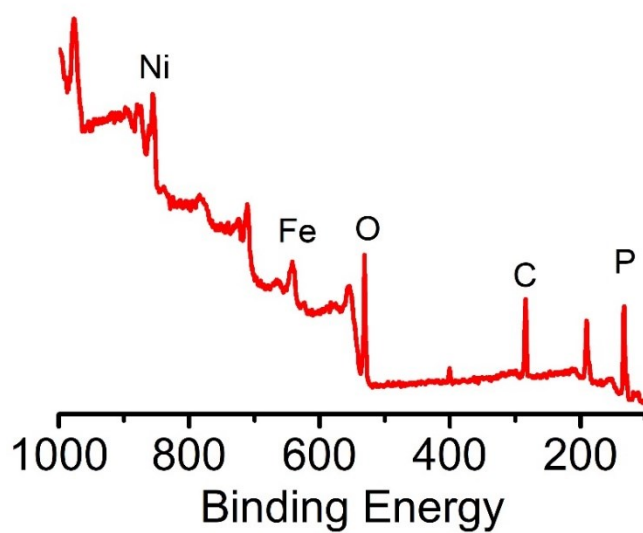
*Calculation of ECSA.* The electrochemically active surface area (ECSA) of the electrocatalyst is evaluated by measurement of their double layer charging capacitance. Briefly, a potential range where no apparent Faradaic process occurred was determined firstly using CV. The charging current ( $i_c$ ) in this potential range was then measured from CV curves at different scan rates.  $C_{DL}$  could be obtained from the slope of the plot of charging currents ( $i_c$ ) vs. scan rates ( $v$ ), eq. 1, which is directly proportional to ECSA.

$$i_c = vC_{DL} \quad (1)$$

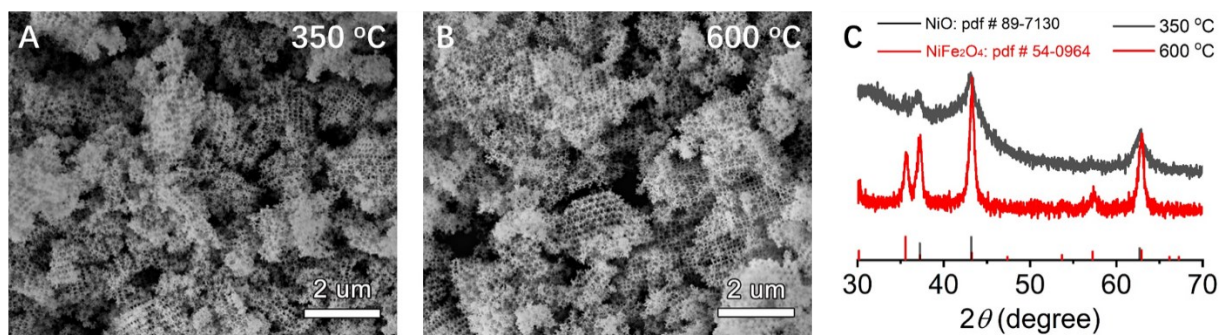
*Electrochemical impedance spectroscopy (EIS).* The EIS was recorded under a given overpotential over a frequency range from 1 MHz to 0.01 Hz at the amplitude of the sinusoidal voltage of 5 mV. The explicit Nyquist plots were obtained based on the EIS data.



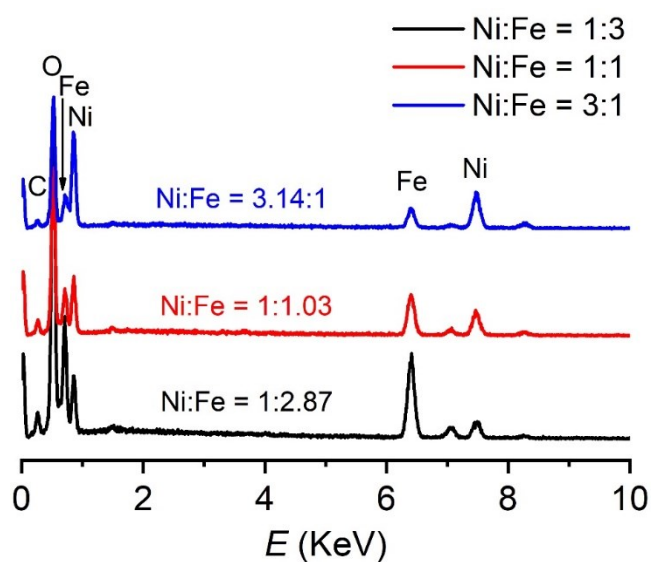
**Figure S1.** (A) N<sub>2</sub> adsorption-desorption isotherms of 3DOM Ni<sub>3</sub>FeO<sub>x</sub> and 3DOM Ni<sub>3</sub>Fe-P. (B) pore size distributions of 3DOM Ni<sub>3</sub>Fe-P calculated from the adsorption curve by the BJH method.



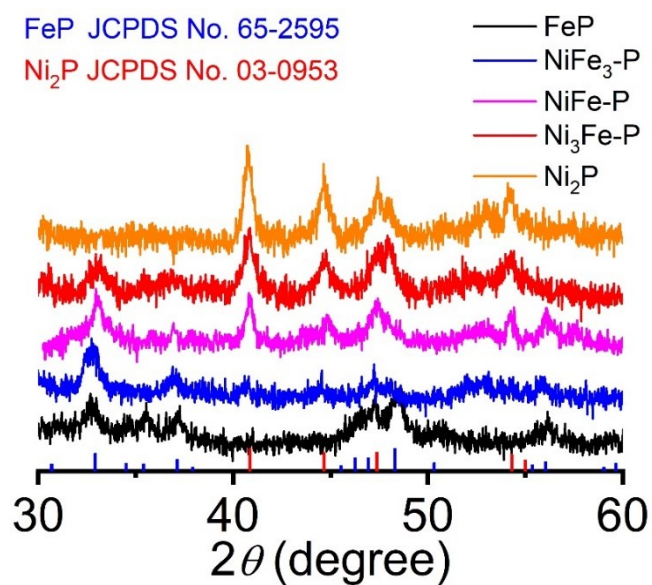
**Figure S2.** The survey XPS spectrum of 3DOM Ni<sub>3</sub>Fe-P.



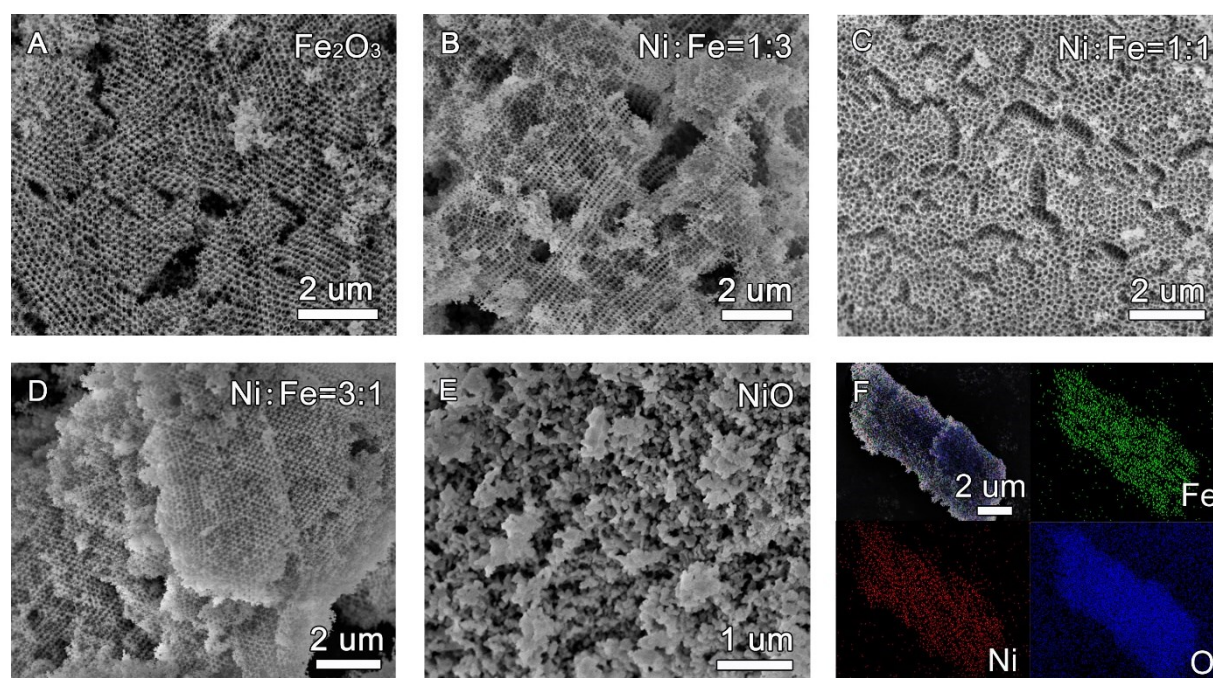
**Figure S3.** (A, B) SEM images of 3DOM  $\text{Ni}_3\text{FeO}_x$  prepared at different pyrolysis temperature and (C) corresponding XRD patterns.



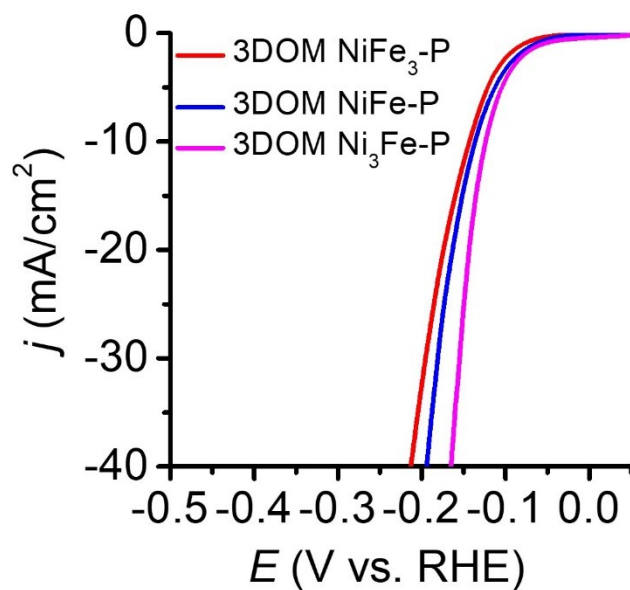
**Figure S4.** SEM-EDX data of different 3DOM NiFe oxide samples with different feeding contents of metal sources during the preparation process.



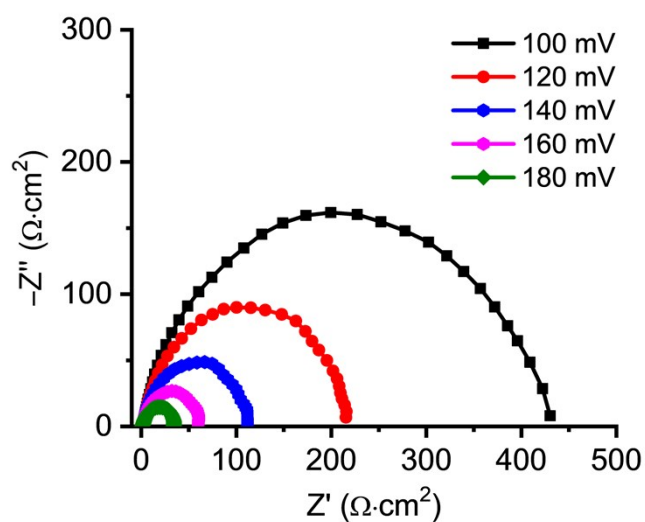
**Figure S5.** XRD patterns of the as-prepared metal phosphide samples as indicated in the figure.



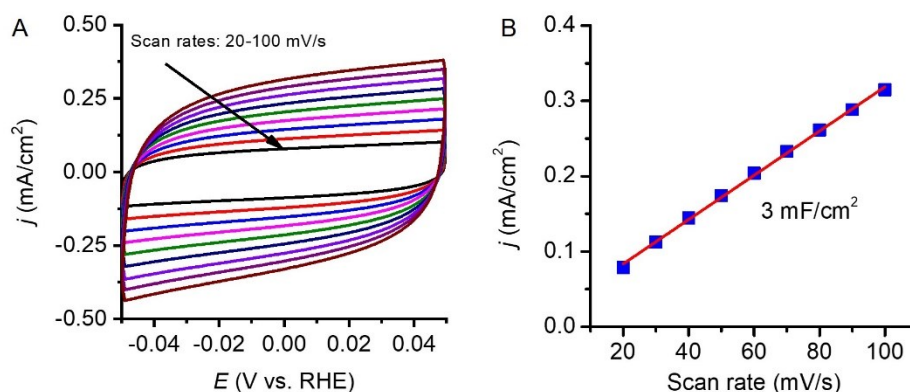
**Figure S6.** SEM images of (A) 3DOM  $\text{Fe}_2\text{O}_3$ , (B) 3DOM  $\text{NiFe}_3\text{O}_x$ , (C) 3DOM  $\text{NiFeO}_x$ , (D) 3DOM  $\text{Ni}_3\text{FeO}_x$ , and (E) NiO NPs. (F) SEM-EDX mapping images of 3DOM  $\text{Ni}_3\text{FeO}_x$ .



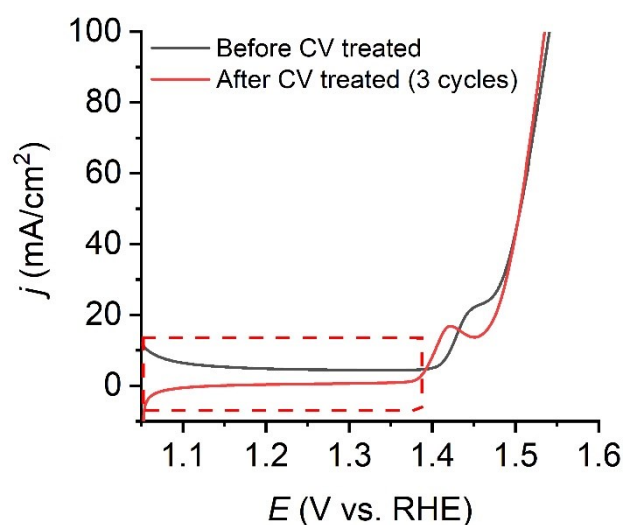
**Figure S7.** LSV curves of 3DOM  $\text{NiFe}_3\text{-P}$ , 3DOM  $\text{NiFe-P}$  and 3DOM  $\text{Ni}_3\text{Fe-P}$  at a scan rate of 2 mV/s in 1 M KOH solution.



**Figure S8.** Nyquist plots of 3DOM  $\text{Ni}_3\text{Fe-P}$  at various overpotentials in 1 M KOH solution for HER.



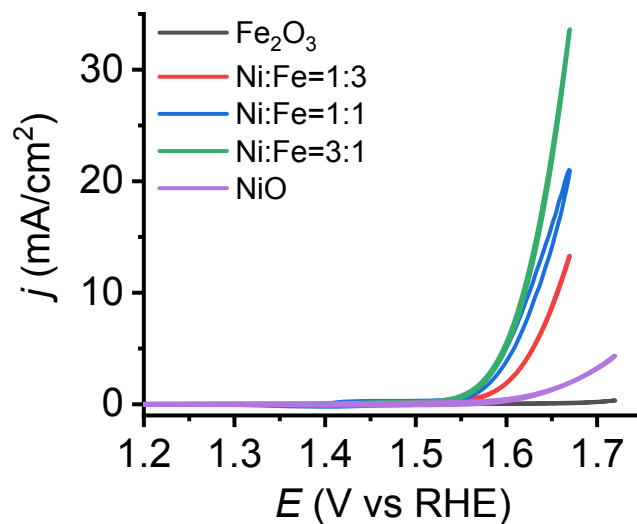
**Figure S9.** (A) Capacitive charging currents of Ni<sub>2</sub>P NPs recorded in the non-Faradaic potential region between -0.05 V – 0.05 V at scan rates from 20 to 100 mV/s at an interval of 10 mV. (B) The anodic charging currents measured at 0 V vs. RHE plotted as a function of scan rates.



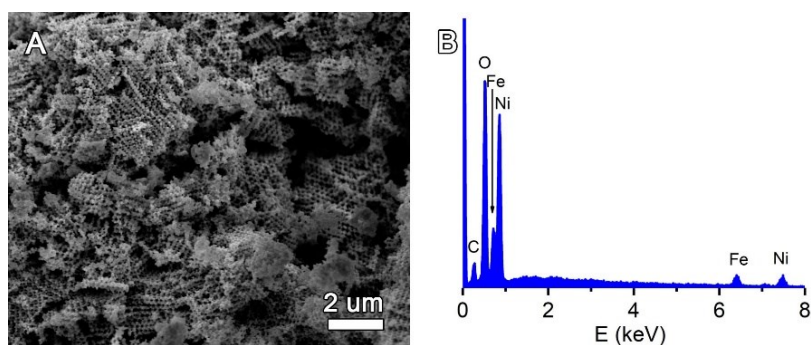
**Figure S10.** LSV plots of 3DOM Ni<sub>3</sub>Fe-P before and after 3-cycle CV treatment for OER in 1 M KOH solution at a scan rate of 2 mV/s.

Figure S10 shows the LSV plots for the untreated and CV-treated 3DOM Ni<sub>3</sub>Fe-P electrodes in 1 M KOH solution. The 3DOM Ni<sub>3</sub>Fe-P electrode without CV treatment exhibits an anodic current density of ~5 mA/cm<sup>2</sup> between 1.1 V - 1.4 V vs. RHE, resulted from surface oxidation of

the phosphides to (oxy)hydroxides. In contrast, the electrode with CV treatment of 3 cycles exhibits only a small double-layered capacitance charging current in the same potential range, with no evidence of surface oxidation.



**Figure S11.** CV curves of NiO NPs, 3DOM Fe<sub>2</sub>O<sub>3</sub> and various 3DOM NiFe oxides in 1 M KOH solution for OER.



**Figure S12.** (A) SEM image and (B) SEM-EDX data of 3DOM Ni<sub>3</sub>Fe-P after 10 h electrolysis for OER in 1 M KOH solution.

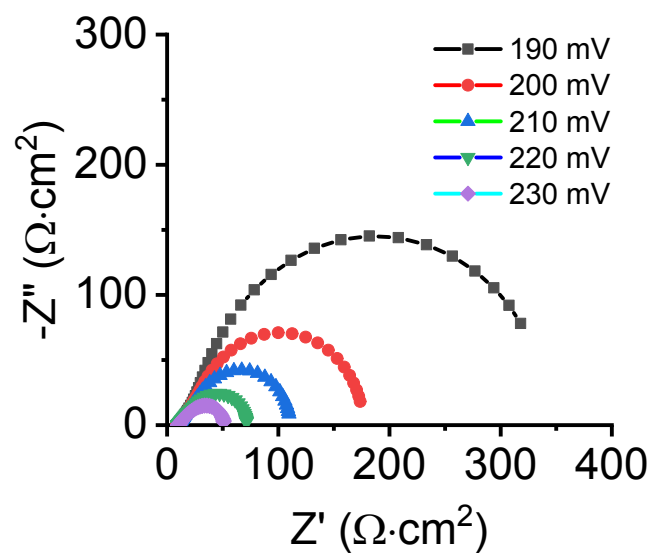


**Figure S13.** Nyquist plots of 3DOM Ni<sub>3</sub>Fe-P at various overpotentials in 1 M KOH solution for OER.

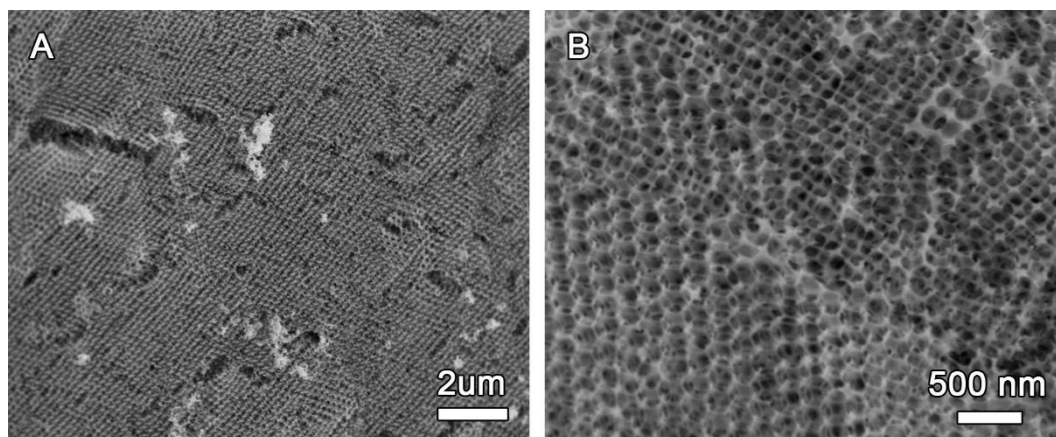


**Figure S14.** SEM images of 3DOM CoFeO<sub>x</sub> at (A) low and (B) high magnifications.

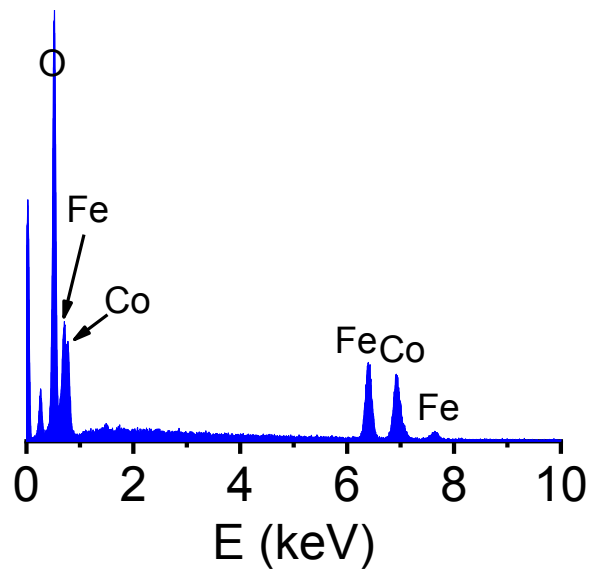


**Figure S15.** SEM-EDX data of 3DOM  $\text{CoFeO}_x$ .

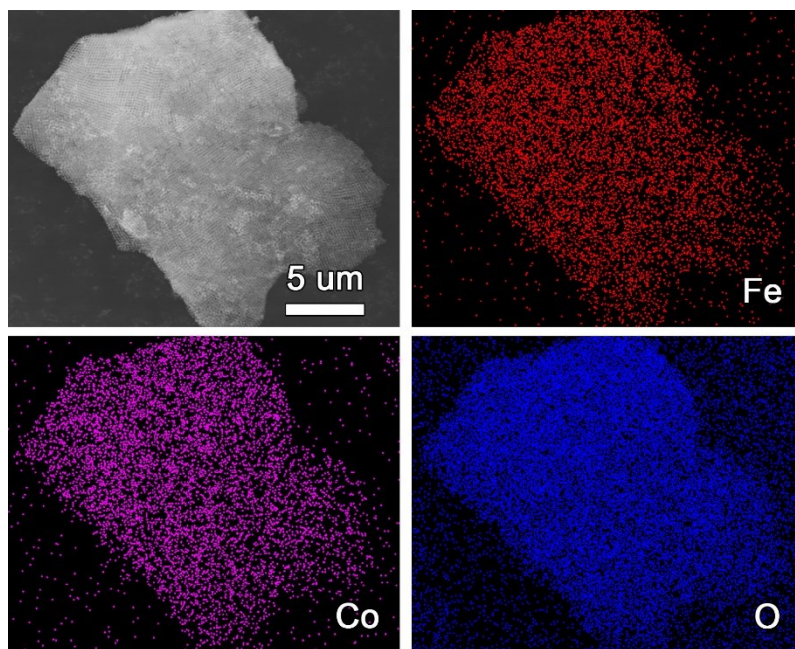


**Figure S16.** SEM and the corresponding SEM-EDX mapping images of 3DOM  $\text{CoFeO}_x$ .

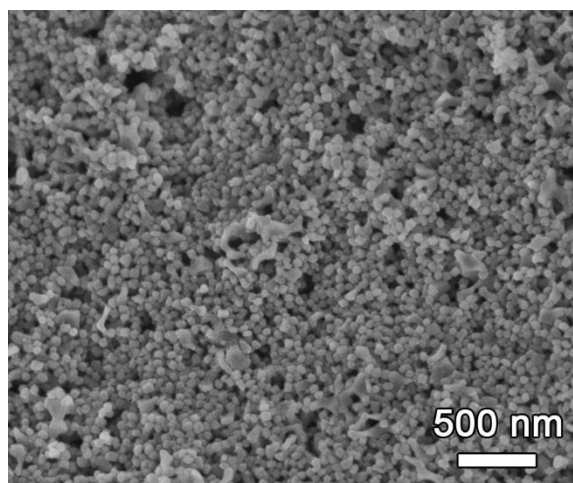


**Figure S17.** SEM images showing that  $\text{CoO}_x$  NPs were obtained by the same template method.

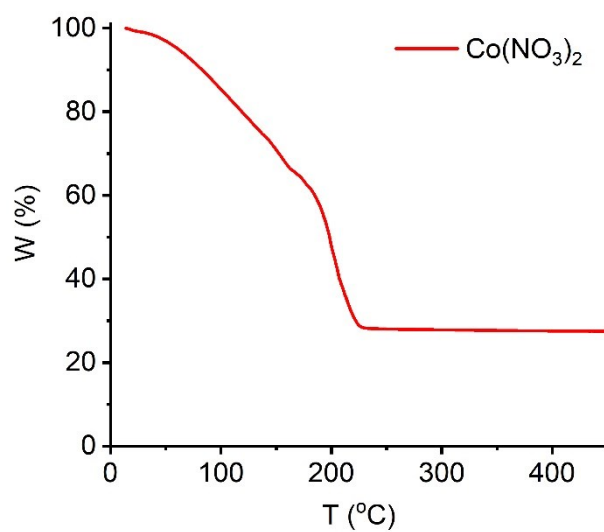


**Figure S18.** TGA curve of  $\text{Co}(\text{NO}_3)_2 \cdot 6\text{H}_2\text{O}$  at a heating rate of 1 °C/min in air.

**Table S1.** Comparison of HER activities of the 3DOM Ni<sub>3</sub>Fe-P and some recently reported metal phosphide catalysts in 1 M KOH solution.

Catalysts	Current density (mA cm <sup>-2</sup> )	Overpotential (mV)	Tafel slope (mV dec <sup>-1</sup> )	Ref.
Co <sub>2</sub> P/CoNPC	10	208	83.9	1
Ni-doped FeP/C	10	95	72	2
Cu <sub>0.3</sub> Co <sub>2.7</sub> P/NC	10	220	122	3
honeycomb NiCoFeP nanosphere	10	149	108	4
hollow porous NiCoFeP nanocubes	10	156	56	5
Ni-Fe-P-350 nanocube	10	183	85	6
Ni <sub>0.69</sub> Co <sub>0.31</sub> P yolk-shell sphere	10	167	47	7
NiCoP/rGO	10	209	124	8
<b>3DOM Ni<sub>3</sub>Fe-P</b>	<b>10</b>	<b>120</b>	<b>61</b>	<b>This work</b>

**Table S2.** Comparison of OER activities of the 3DOM Ni<sub>3</sub>Fe-P and some recently reported metal phosphide catalysts in 1 M KOH solution.

Catalysts	Current density (mA cm <sup>-2</sup> )	Overpotential (mV)	Tafel slope (mV dec <sup>-1</sup> )	Ref.
honeycomb NiCoFeP nanosphere	10	270	65	4
hollow porous NiCoFeP nanocubes	10	295	35	5
FeCo-P/C Nanocomposites	10	362	50.1	9
CNTs@NiCoP/C composite	10	297	57.3	10
NiCoP/C nanoboxes	10	330	96	11
(Ni <sub>0.62</sub> Fe <sub>0.38</sub> ) <sub>2</sub> P hollow nanocubes	10	290	44	12
Ni <sub>0.6</sub> Co <sub>1.4</sub> P nanocages	10	300	80	13
CoP nanoframes	10	323	49.6	14
Co <sub>0.4</sub> Fe <sub>0.28</sub> P nanocubes	10	270	25.6	15
NiFeP@NPC	10	350	78	16
Ni <sub>2</sub> P-CoP	10	320	69	17
<b>3DOM Ni<sub>3</sub>Fe-P</b>	<b>10</b>	<b>230</b>	<b>40</b>	<b>This work</b>

## Supplementary References

- 1 H. Liu, J. Guan, S. Yang, Y. Yu, R. Shao, Z. Zhang, M. Dou, F. Wang and Q. Xu, *Adv. Mater.*, 2020, 2003649.
- 2 X. F. Lu, L. Yu and X. W. D. Lou, *Sci. Adv.*, 2019, **5**, eaav6009.
- 3 J. Song, C. Zhu, B. Z. Xu, S. Fu, M. H. Engelhard, R. Ye, D. Du, S. P. Beckman and Y. Lin, *Adv. Energy Mater.*, 2017, **7**, 1601555.
- 4 X. Wei, Y. Zhang, H. He, L. Peng, S. Xiao, S. Yao and P. Xiao, *Chem. Commun.*, 2019, **55**, 10896-10899.
- 5 Y. Guo, J. Tang, Z. Wang, Y. Sugahara and Y. Yamauchi, *Small*, 2018, **14**, 1802442.
- 6 C. Xuan, J. Wang, W. Xia, Z. Peng, Z. Wu, W. Lei, K. Xia, H. L. Xin and D. Wang, *ACS Appl. Mater. Interfaces*, 2017, **9**, 26134-26142.
- 7 Z. Yin, C. Zhu, C. Li, S. Zhang, X. Zhang and Y. Chen, *Nanoscale*, 2016, **8**, 19129-19138.
- 8 G. Zhang, G. Wang, Y. Liu, H. Liu, J. Qu and J. Li, *J. Am. Chem. Soc.*, 2016, **138**, 14686-14693.
- 9 W. Hong, M. Kitta and Q. Xu, *Small Methods*, 2018, **2**, 1800214.
- 10 Y. Zhao, G. Fan, L. Yang, Y. Lin and F. Li, *Nanoscale*, 2018, **10**, 13555-13564.
- 11 P. He, X. Y. Yu and X. W. Lou, *Angew. Chem. Int. Ed. Engl.*, 2017, **56**, 3897-3900.
- 12 H.-H. Zou, C.-Z. Yuan, H.-Y. Zou, T.-Y. Cheang, S.-J. Zhao, U. Y. Qazi, S.-L. Zhong, L. Wang and A.-W. Xu, *Catal. Sci. Technol.*, 2017, **7**, 1549-1555.
- 13 B. Qiu, L. Cai, Y. Wang, Z. Lin, Y. Zuo, M. Wang and Y. Chai, *Adv. Funct. Mater.*, 2018, **28**, 1706008.
- 14 L. Ji, J. Wang, X. Teng, T. J. Meyer and Z. Chen, *ACS Catal.*, 2019, **10**, 412-419.
- 15 Z. Cao, T. Zhou, W. Xi and Y. Zhao, *Electrochim. Acta*, 2018, **263**, 576-584.
- 16 J. Wang and F. Ciucci, *Appl. Catal., B: Environ.*, 2019, **254**, 292-299.
- 17 X. Liang, B. Zheng, L. Chen, J. Zhang, Z. Zhuang and B. Chen, *ACS Appl. Mater. Interfaces*, 2017, **9**, 23222-23229.